Transient creep, aseismic damage and slow failure in Carrara marble deformed across the brittle-ductile transition

A. Schubnel,[1] E. Walker,[2] B. D. Thompson,[1] J. Fortin,[3] Y. Guéguen,[3] and R. P. Young[1]

Received 18 April 2006; revised 24 June 2006; accepted 12 July 2006; published XX Month 2006.

[1] Two triaxial compression experiments were performed on Carrara marble at high confining pressure, in creep conditions across the brittle-ductile transition. During cataclastic deformation, elastic wave velocity decrease demonstrated damage accumulation (microcracks). Keeping differential stress constant and reducing normal stress induced transient creep events (i.e., fast accelerations in strain) due to the sudden increase of microcrack growth. Tertiary creep and brittle failure followed as damage came close to criticality. Coalescence and rupture propagation were slow (60–200 seconds with ∼150 MPa stress drops and millimetric slips) and radiated little energy in the experimental frequency range (0.1–1 MHz). Microstructural analysis pointed out strong interactions between intra-crystalline plastic deformation (twinning and dislocation glide) and brittle deformation (microcracking) at the macroscopic level. Our observations highlight the dependence of acoustic efficiency on the material's rheology, at least in the ultrasonic frequency range, and the role played by pore fluid diffusion as an incubation process for delayed failure triggering. **Citation:** Schubnel, A., E. Walker, B. D. Thompson, J. Fortin, Y. Guéguen, and R. P. Young (2006), Transient creep, aseismic damage and slow failure in Carrara marble deformed across the brittle-ductile transition, *Geophys. Res. Lett.*, *33*, LXXXXX, doi:10.1029/2006GL026619.

1. Introduction

[2] Interest in the brittle-ductile transition has increased considerably in recent years, in large part due to the fact that the maximum depth of seismicity corresponds to a transition in the crust and in the upper mantle from seismogenic brittle failure to aseismic cataclastic flow, that is, from localized to homogeneous deformation. The mechanics of the transition depends both on extrinsic variable (state of solid stress, pore pressure, temperature, fluid chemistry and strain rate) and intrinsic parameters (modal composition of the rock, porosity, crack and dislocation density) [*Paterson and Wong*, 2005]. The deformation mechanisms operative during the transition occur on scales ranging from microscopic to macroscopic and have profound influence on the spatiotemporal evolution of stress and deformation [*Du et al.*, 2003], as well as in the coupling of crustal deformation and fluid transport [*Miller*, 2002]. Thus, investigating the interplay between intragranular plasticity and cracking in the laboratory may be critical in order to understand the mechanics of the lower seismogenic zone and/or the early stages of earthquake nucleation [*Rice and Cocco*, 2006].

[3] In the laboratory, marbles have been studied widely for they can undergo a brittle-plastic transition at room temperature as calcite requires low shear stresses to initiate plastic processes: *r*-, *f*-dislocation glide and twinning are activated even at room temperature [*Turner et al.*, 1954]. A number of these studies have documented the mechanical behavior of Carrara marble [*Rutter*, 1974; *Fredrich et al.*, 1989; *Renner et al.*, 2002; *Schubnel et al.*, 2005]. In the cataclastic flow regime, it was demonstrated that deformation is dominated by dislocation creep [*Renner et al.*, 2002], twinning and cracking [*Fredrich et al.*, 1989]. *Schubnel et al.* [2005] showed that the interactions between plastic deformation and brittle processes induced the pore space to either dilate (in creep) or compact (in pure relaxation), without any strain localization taking place. In the present study, two triaxial experiments were performed at room temperature, across the brittle-ductile transition, until failure was finally triggered, in wet and dry conditions respectively.

2. Experimental Set-Up and Procedure

[4] Two cylindrical samples of Carrara marble (length = 80mm, diameter = 40mm) were deformed in a triaxial cell installed at Ecole Normale Supérieure [*Schubnel et al.*, 2005]. 2:1 ratio samples were used because of space limitation inside the pressure vessel. This cell is equipped to record strain, permeability, elastic wave velocities and acoustic activity contemporaneously. A network of 14 piezoceramic transducers (PZT, eigen frequency 1 MHz) was used in order to measure P wave velocities along several directions. Relative error was 0.5% using cross-correlation and double picking techniques, while the absolute error was of the order of a few percents (1–2%). Acoustic Emission (AE) activity was captured using a unique instrument [*Thompson et al.*, 2005, 2006], which stores continuous ultrasonic waveform data onto a 40 GB circular Random Access Memory (RAM) buffer at 10 MHz sampling frequency. The RAM was frozen a few seconds after macroscopic rupture.

[5] Inside the vessel, the samples were covered with a neoprene jacket and oil resistant silicon for insulation. Cumulative axial strain was measured using a LVDT located outside the vessel, on top of the piston. Pore pressure was driven by two precision volumetric pumps and water was introduced into the sample through hardened steel end pieces located on the top and bottom of the rock sample. Experiments were performed at room temperature, under wet and dry conditions (termed AeWet and AeDry respectively), using constant stress ramps of ∼1 MPa.minP^{-1P}. The wet sample was saturated for

[1]Lassonde Institute, University of Toronto, Toronto, Ontario, Canada.
[2]Ecole et Observatoire des Sciences de la Terre, Strasbourg, France.
[3]Laboratoire de Geologie, Ecole Normale Superieure, Paris, France.

0094-8276/06/2006GL026619$05.00

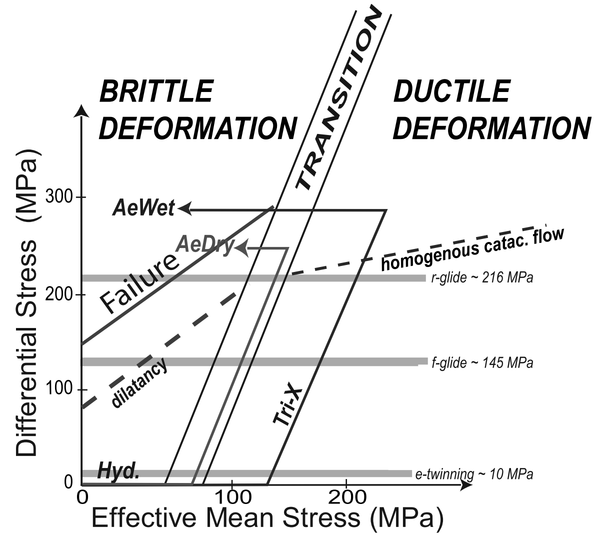

Figure 1. Stress path followed during experiments AeWet and AeDry as a function of differential stress $(\sigma B_{1B} - \sigma B_{3B})$ and effective mean stress $(\sigma B_{1B} + 2\sigma B_{3B})/3 - PB_{pB}$. Onsets of dilatancyP^{P} and homogeneous dilatant cataclastic flow in Carrara marble [from *Schubnel et al.*, 2005], e-twinning, f and r- dislocation in calcite single crystalsP^{P} [from *Turner et al.*, 1954] are displayed on the figure.

24 hours prior to the experiment and then deformed under drained conditions.

[6] A number of studies have already documented the mechanical behavior of Carrara marble along regular triaxial path [*Rutter*, 1974; *Fredrich et al.*, 1989; *Renner et al.*, 2002; *Schubnel et al.*, 2005]. These studies showed that below 50 MPa confinement, deformation is brittle. At higher confinement, cataclastic flow takes place, accompanied by strain hardening [*Fredrich et al.*, 1989], damage is homogenous and strain localization does not take place, even at very large strains [*Schubnel et al.*, 2005]. For such reasons, particular stress paths across the brittle-ductile transition were chosen for this study (Figure 1). For AeWet, confining pressure Pc and pore pressure Pp were initially set to 125 MPa and 5 MPa respectively. After irreversible plastic hardening (∼5% plastic axial strain) in the cataclastic flow regime, the sample was brought back at constant differential stress ($\sigma 1 - \sigma 3$ = 290 MPa) into the brittle field by increasing pore pressure (Pp) so that the remaining effective confinement ($PB_{\text{eff B}}$ = Pc − Pp) was equal to 5MPa. Because no AE activity was observed during this first experiment performed in the wet regime, a second experiment, AeDry, was performed at lower confining pressure, in dry conditions: AeDry sample was initially subjected to 75 MPa confining pressure and 250 MPa differential stress. The confining pressure was then slightly decreased.

3. Experimental Results

[7] Figure 2a plots the evolution of differential stress, effective confining pressure, axial strain and P wave velocity with time during AeWet. The onset of plastic deformation was reached at a differential stress value of ∼150 MPa. From this point, elastic wave velocities decreased rapidly which reveals important damage accumulation. On the contrary, P wave anisotropy increased, which indicates crack propagated along preferential orientations (sub-axial).

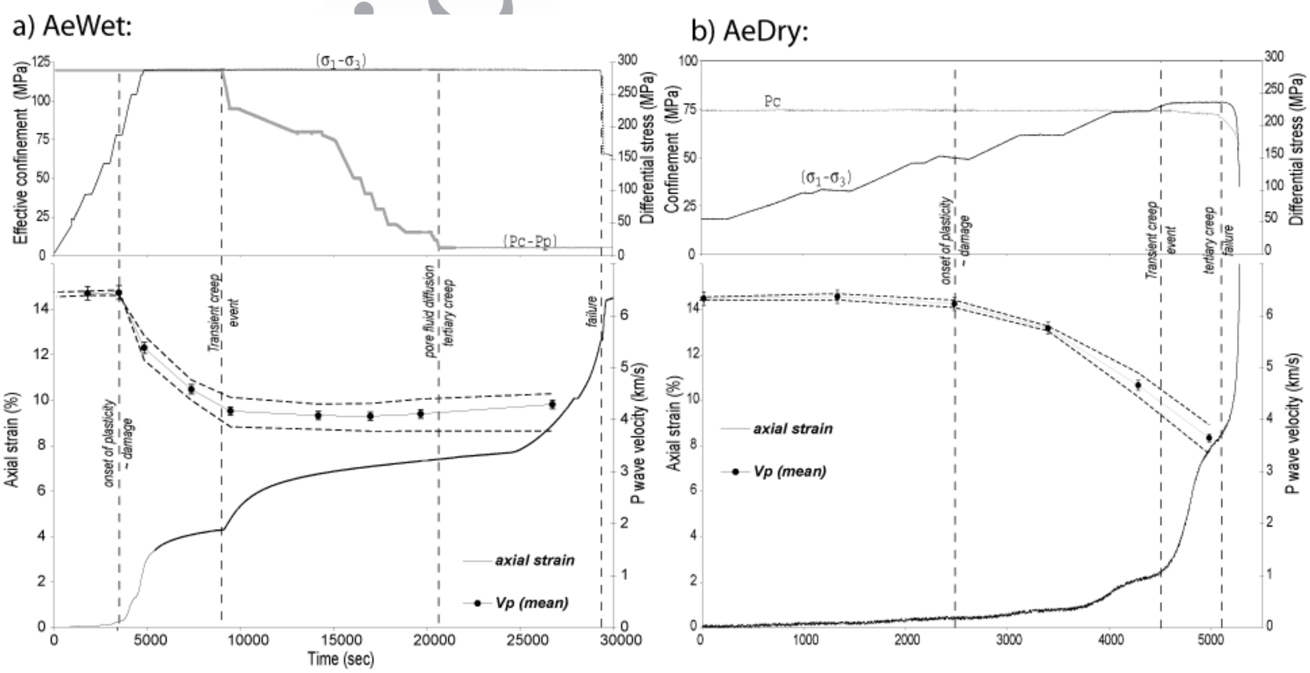

Figure 2. Evolution of differential stress, effective confining pressure, axial strain and P wave velocities vs. time in experiments (a) AeWet and (b) AeDry. Variations in the stress conditions are indicated on the top of the figure ($\sigma 1 - \sigma 3$ = differential stress, Pc = confining pressure, $PB_{cB} - PB_{pB}$ = effective confining pressure). Symbols correspond to the mean value of P wave velocities, whereas dashed lines highlight the anisotropy (vertical P wave is fast, horizontal P wave is slow). Transient creep events, onsets of plastic deformation, tertiary creep and failure are indicated.

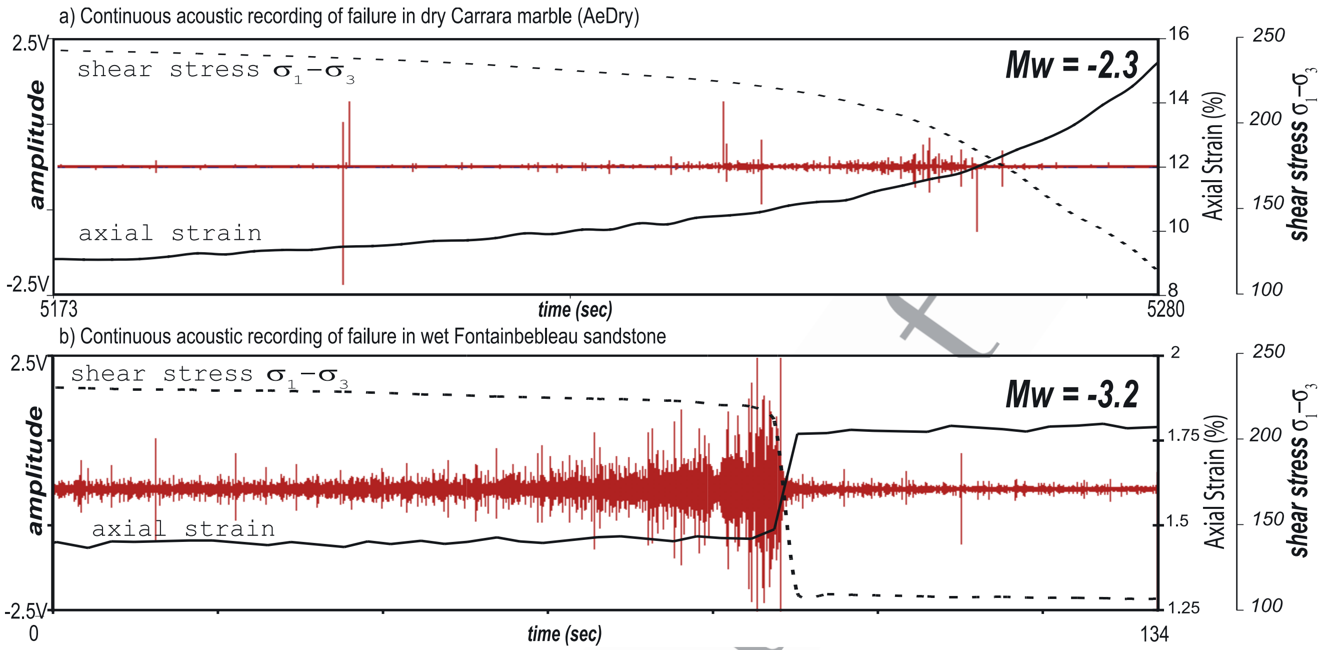

Figure 3. Stress, strain and radiated acoustic energy (frequency range = 0.1–1 MHz). (a) In AeDry: evolution of axial strain, shear stress and acoustic activity (107 seconds segment of the continuous waveform recorded at failure) versus time. (b) In an intact Fontainebleau sandstone (134 seconds continuous waveform recorded at failure). Stress scale is the same in Figures 3a and 3b, not strain scale. Moment magnitudes MB_{WB}, calculated from the mechanical data, are indicated for comparison.

As the effective confining stress was lowered at constant differential stress ($\sigma1 - \sigma3 = 290$ MPa), a fast acceleration in axial strain was observed. This is thought to be due to a rapid increase in the growth of the existing microcracks, which were destabilized as normal stress was suddenly lowered. A few hours after the effective confining pressure reached its minimal value of 5 MPa, the sample eventually entered tertiary creep. After 12% cumulative axial shortening and one hour after the sample entered tertiary creep, brittle failure finally occurred. The 150 MPa stress drop was released over approximately 200 seconds. Unlike in purely brittle materials, no acoustic emission activity was associated to damage and brittle failure.

[8] At lower confinement (75 MPa) and in dry conditions (Figure 2b), the onset of plasticity was reached at ~175 MPa differential stress. From this point, P wave velocities decreased by over 50%, indicating a rapid accumulation of damage. A rapid increase in anisotropy was also observed beyond the onset of plasticity, reaching 15% prior to brittle failure, which remains low when compared to that observed on dry granite samples deformed in the brittle field [*Stanchits et al.*, 2003; *Schubnel et al.*, 2003]. A small decrease (5 MPa) of confinement was sufficient to almost instantaneously trigger a large transient creep event, followed by brittle rupture. This time, time delay to failure was much shorter (of the order of a few minutes) and again, damage accumulation and failure initiation triggered no acoustic emissions. The stress drop was released in approximately 60 seconds.

[9] The slips were ~1.5 mm and 5 mm in the AeWet and AeDry respectively. Considering a 60 P^{oP} dipping fault, this yields seismic moments MB_{0B} (calculated as $MB_{0B} = \mu\, Au$, with shear modulus, $\mu = 20$ GPa, fault area $A = 29$ cmP^{2P} and u as the measured slip) equal to $\sim 1 \times 10$P^{5P} and 3×10P^{5} ^{P}Nm, which corresponds to moment magnitudes (MB_{WB}, calculated using $MB_{WB} = 2/3\ \log B_{10\ B} MB_{0B} - 6.0$) of approximately -2.3 and -2.6 respectively. The continuous acoustic waveform recorded at rupture in AeDry (Figure 3a) shows that the peak differential stress cannot be correlated to any particular acoustic emissions. Brittle failure therefore seems to have initiated aseismically (at least in the ultrasonic experimental frequency range, i.e., 0.1–1 MHz). One should note however that, as the slip accelerated during the latter phase of rupture propagation and/or frictional sliding, the amount of recorded acoustic activity increased, which might be due to the shearing of asperities. In any case, rupture radiated very little energy compared to what is typically observed on intact silicastic rocks such as granites [*Thompson et al.*, 2006].

4. Discussion

[10] For comparison, Figure 3b displays an example of the acoustic activity recorded at failure in an intact Fontainebleau sandstone deformed in similar conditions. The recorded energy is one and a half orders of magnitude larger than for the AeDry sample, although the calculated moment magnitude is equal to -3.2 (equivalent to a 200 μm slip), that is, almost one order of magnitude lower. Attenuation and scattering, larger in the sandstone, cannot be responsible of the major differences in the two recordings. However, these differences can be qualitatively understood when considering that: 1) the fracture toughness of quartz (~1 MPa.mP$^{1/2P}$) is one order of magnitude larger than that of calcite (~0.2 MPa.mP$^{1/2P}$) [*Atkinson and Avdis*, 1980];

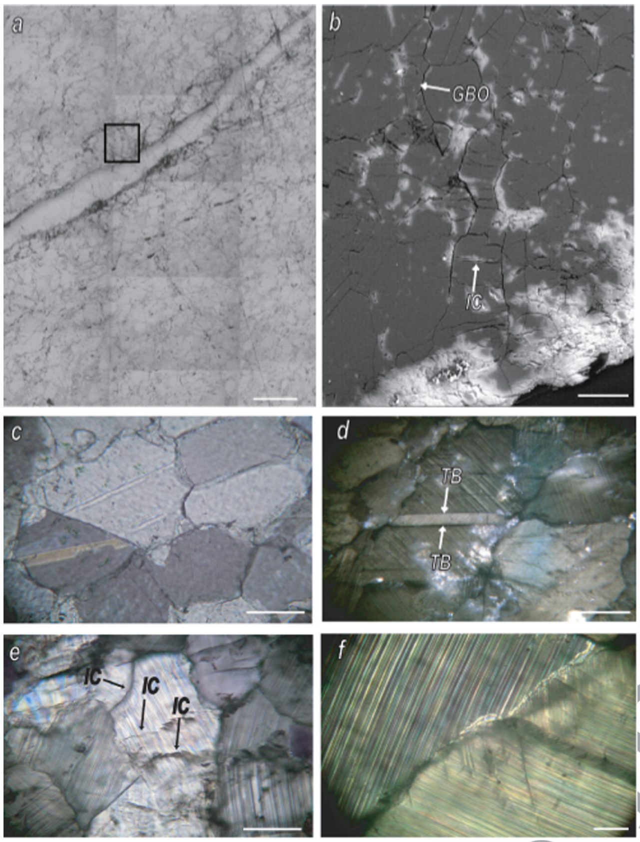

Figure 4. Microstructural analysis. Sections were taken in the horizontal plane, perpendicular to the compression axis. (a) Mosaic image of fractured AeWet sample in reflected light. (b) A SEM image of the fracture wall and its vicinity; the box indicates the location of Figure 1b. (c) Cross-polarized image of an undeformed sample. (d–f) Cross polarized images of the deformed sample, AeWet, far from the rupture plane. The white scale corresponds to 1mm in Figure 4a; 100 μm in Figure 4b–4e; 20 μm in Figure 4f. IC = intragranular cracks, GBO = grain boundary opening, TB = thick twin boundary.

2) in the case of a purely brittle material such as Fontainebleau sandstone, the stress drop is released instantaneously (<1 second) and the maximum radiated acoustic energy clearly correlates to the peak stress. This last observation clearly highlights the dependence of acoustic (and seismic?) efficiency not only on the rupture propagation speed and the slip velocity but also on the rock's rheology.

[11] Figure 4 presents a series of micrographs of the fracture plane, which was oriented at ~45 degrees from the vertical. Thin sections were made in a plane perpendicular to the compression axis, in order to show the extent of the process zone around the main fracture. Figure 4a is a mosaic in reflected light of the fractured sample AeWet. The failure plane is narrow (two to three grain diameters wide), not so rough and filled with very fine gouge material. Only few intergranular fractures can be observed near the fracture plane (Figure 4b) and the process zone is narrow (~<100 μm). Figure 4c shows micrographs of an intact (un-damaged) sample of Carrara marble, while Figures 4d, 4e and 4f show the deformed AeWet sample, in cross-polarized light. In the intact marble (Figure 4c), few twins are present initially and grain boundaries are sealed. In the deformed sample, most of the shear deformation was accommodated by the presence of mechanical twins at very high density (Figures 4d, 4e and 4f). Strong interactions between microcracking and twinning can be observed, as the bending of twins can nucleate intragranular cracks (Figure 4e) or induce grain boundary opening (Figures 4b and 4d). In our experiments, twinning is pervasive at very high density in all grains (Figure 4f). We observe a preferential crack nucleation at grain boundaries and twin intersections which suggest that microcracking could be caused by dislocation pile-ups (Figure 4d).

[12] In calcite bearing rocks and at low temperature, competition between two basic micromechanisms (mode I cracking and dislocation glide), controls the macroscopic behavior (brittle versus ductile). Twinning and dislocation glide are intra-crystalline processes not sensitive to pressure, whereas mode I cracking is pressure-sensitive. Twinning is particularly important when only a limited number of slip systems are activated in a crystal, as it can palliate the need of five independent glide systems required for plastic deformation to take place in any direction [*Paterson and Wong*, 2004]. But twin boundaries are obstacles to dislocation glide and randomly oriented grains can only twin along certain preferential crystallographic directions. This gives rise to elastic strain incompatibilities and microcracks are needed in order to accommodate plastic deformation. Both for AeWet and AeDry, the evolution of crack density was calculated from P wave velocities evolution (Figure 2) using two well-established Effective Medium theories: the Non-Interacting Cracks [*Kachanov*, 1994] and the Extended Differential Self-Consistent (DEM) [*Le Ravalec and Guéguen*, 1996] methods. The DEM has been proven to be the most reliable method to calculate the effective elastic properties of cracked rocks [*Orlowsky et al.*, 2003] as it takes into account the existing stress interactions between cracks. However, the non-interacting crack theory, which neglects stress interactions, is particularly relevant here as intragranular plasticity tends to inhibit long range stress interactions. Using matrix Young's modulus and Poisson's ratio as that of pure calcite, that is, 100 GPa and 0.32 respectively, a fluid bulk modulus equal to that of water, that is, 2 GPa, P-wave velocities were inverted directly into crack density using a simple least square fit (see *Schubnel et al.* [2003, 2006] for details of the inversion method). Figure 5 illustrates that both inversions (the DEM and the NIC) give comparable results. Initially, the crack density decreased from ~0.15 to ~0.1 as effective mean stress $(\sigma B_{1B} + 2\sigma B_{3B})/3 - PB_{pB}$ increased, which is synonym of crack closure. Beyond the onset of plasticity, crack density increased suddenly due to microcrack nucleation and propagation. At failure, crack density reached values comprised between 0.7 and 1; 1 being the theoretical percolation threshold for macroscopic failure in 3 dimensions [*Guéguen et al.*, 1997]. Brittle failure aroused when damage was close to a critical value, which is consistent with the works of *Baud and Meredith* [1997] on Darley Dale sandstone. On the other hand, the time delay to failure in the wet experiment is thought to correspond to the time for pore pressure to diffuse throughout the sample. Such a

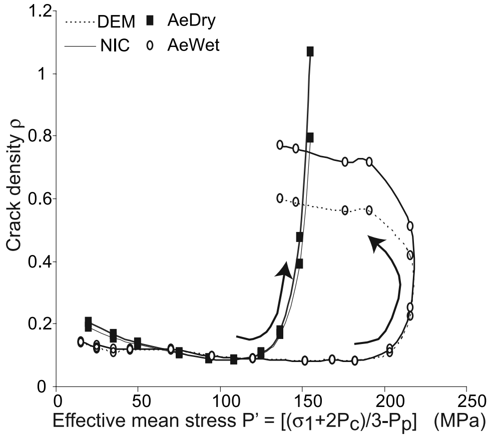

Figure 5. Evolution of the crack density using the Non-Interacting Cracks theory (NIC – solid lines) [*Kachanov*, 1994] and the Extended Differential Self-Consistent method (DEM – dashed lines) [*Le Ravalec and Guéguen*, 1996]. Wet (plain symbols) and dry (empty symbols) P-wave velocities (Figures 2a and 2b) were inverted into crack density using both methods (see *Schubnel et al.* [2003, 2006] for details of the inversion method). Matrix Young's modulus and Poisson's ratio were taken equal 100 GPa and 0.32 respectively, fluid bulk modulus equal to 2 GPa.

hypothesis yields a hydraulic diffusivity D of $\sim$10P^{-8P} mP^{2P}.sP^{-1P}, equivalent to a permeability of k $\sim$ 10P$^{-20\ P}$ mP^{2P}. This is consistent with our crack density analysis [*Schubnel et al.*, 2006], the experimental determination of Carrara marble's permeability at high pressure [*Zhang et al.*, 1994] and the determination of real fault gouge permeabilities [*Wibberley and Shimamoto*, 2003].

5. Conclusions and Implications

[13] When the confining pressure is sufficient to prevent mode I cracking, damage in Carrara marble is intra-crystalline with twinning and dislocations piling up (as in a cold worked metal). Because of the low temperatures, dislocation and twin accumulation is such that cracks are needed in order to accommodate local plastic differential strain mismatches. Lowering the normal stress can induce a short-lived fast acceleration in strain (i.e., transient creep event), due to the sudden growth of destabilized microcracks. However, crack propagation steps radiate small amounts of energy in the experimental frequency range (0.1 – 1 MHz), due to the low surface energy of calcite. Radiated energy might also have been absorbed by neighboring dislocations [*Lawn*, 1993] and/or intermittent dislocation flow [*Weiss and Marsan*, 2003]. When the crack density becomes close to a critical value of 1, crack coalescence and slow brittle failure takes place.

[14] Our work clearly highlights the dependence of the ultrasonic (and seismic?) acoustic efficiency not only on the rupture propagation speed and the slip velocity but also the rock's rheology. It also illustrates the possible role played by pore fluid diffusion as an incubation process for delayed failure triggering. While in the laboratory, this could have implications for the mechanics of the lower seismogenic zone [*Du et al.*, 2003]. There, ductile minerals prevalent in Earth's crust, such as quartz and feldspar are predicted to behave in a similar fashion above 300°C as calcite does at room temperature [*Tullis and Yund*, 1992]. Within fault gouges and even at shallower depths, clays might also behave the same way.

[15] **Acknowledgments.** The authors would like to thank P. Benson, M. H. B. Nasseri, D. Collins and the many researchers who, through numerous discussions, helped to greatly improve this manuscript. This research was funded via a National Environment Research Council (NERC) equipment grant, a Natural Sciences and Engineering Research Council of Canada (NSERC) Discovery Grant and the Fond France Canada pour la Recherche (FFCR). We would also like to thanks three anonymous reviewers, who helped to greatly improve this manuscript.

References

Atkinson, B. K., and V. Avdis (1980), Fracture mechanics parameters of some rock deforming minerals determined using an indentation technique, *Int. J. Rock Mech. Min. Sci., Geomech. Abstr.*, *17*, 383 – 386.

Baud, P., and P. B. Meredith (1997), Damage accumulation during triaxial creep of Darley Dale sandstone from pore volumometry and acoustic emission, *Int. J. Rock Mech. Min. Sci.*, *34*, 024.

Du, W., L. R. Sykes, B. E. Shaw, and C. H. Scholz (2003), Triggered aseismic fault slip from nearby earthquakes, static or dynamic effect?, *J. Geophys. Res.*, *108*(B2), 2131, doi:10.1029/2002JB002008.

Fredrich, J. T., B. Evans, and T.-F. Wong (1989), Micromechanics of the brittle to plastic transition in Carrara marble, *J. Geophys. Res.*, *94*, 4129 – 4145.

Guéguen, Y., T. Chelidze, and M. Le Ravalec (1997), Microstructures, percolation thresholds, and rock physical properties, *Tectonophysics*, *279*, 23 – 35.

Kachanov, M. (1994), Elastic solids with many cracks and related problems, *Adv. Appl. Mech.*, *30*, 259 – 445.

Lawn, B. R. (1993), U*Fracture of Brittle Solids*U, Cambridge Univ. Press, New York.

Le Ravalec, M., and Y. Guéguen (1996), High and low frequency elastic moduli for a saturated porous/cracked rock—Differential self consistent and poroelastic theories, *Geophysics*, *61*, 1080 – 1094.

Miller, S. A. (2002), Properties of large ruptures and the dynamical influence of fluids on earthquakes and faulting, *J. Geophys. Res.*, *107*(B9), 2182, doi:10.1029/2000JB000032.

Orlowsky, B., E. H. Saenger, Y. Guéguen, and S. A. Shapiro (2003), Effects of parallel crack distributions on effective elastic properties—A numerical study, *Int. J. Fract.*, *124*, 171 – 178.

Paterson, M. S., and T.-F. Wong (2005), U*Experimental Rock Deformation: The Brittle Field*, 2Pnd ed., 347 pp., Springer, New York.

Renner, J., B. Evans, and G. Siddiqi (2002), Dislocation creep of calcite, *J. Geophys. Res.*, *107*(B12), 2364, doi:10.1029/2001JB001680.

Rice, J. R., and M. Cocco (2006), Seismic fault rheology and earthquake dynamics, in *The Dynamics of Fault Zones*, edited by M. R. Handy, MIT Press, Cambridge, Mass.

Rutter, E. H. (1974), The influence of temperature, strain rate and interstitial water in the deformation of calcite rocks, *Tectonophysics*, *22*, 331 – 334.

Schubnel, A., O. Nishizawa, K. Masuda, X. J. Lei, Z. Xue, and Y. Guéguen (2003), Velocity masurements and crack density determination during wet triaxial experiments on Oshima and Toki granites, *Pure Appl. Geophys.*, *160*, 869 – 887.

Schubnel, A., J. Fortin, L. Burlini, and Y. Guéguen (2005), Damage and recovery of calcite rocks deformed in the cataclastic regime, in *High Strain Zones*, edited by D. Bruhn and L. Burlini, *J. Geol. Soc. London*, *245*, 203 – 221.

Schubnel, A., P. M. Benson, B. D. Thompson, J. F. Hazzard, and R. P. Young (2006), Quantifying damage, saturation and anisotropy in cracked rocks by inverting elastic wave velocities, *Pure Appl. Geophys.*, *163*, 947 – 973.

Stanchits, S. A., D. A. Lockner, and A. V. Ponomarev (2003), Anisotropic changes in P-wave velocity and attenuation during deformation and fluid infiltration of granite, *Bull. Seismol. Soc. Am.*, *93*, 1803 – 1822.

Thompson, B. D., R. P. Young, and D. A. Lockner (2005), Observations of premonitory acoustic emission and slip nucleation during a stick slip experiment in smooth faulted Westerly granite, *Geophys. Res. Lett.*, *32*, L10304, doi:10.1029/2005GL022750.

Thompson, B. D., R. P. Young, and D. A. Lockner (2006), Observations of fracture in westerly granite under AE feedback and constant strain rate loading: Nucleation, quasi-static propagation, and the transition to unstable fracture propagation, *Pure Appl. Geophys.*, *163*, 995 – 1019.

Tullis, J., and R. A. Yund (1992), The brittle-ductile transition in feldspar aggregates: And experimental study, in U*Fault Mechanics and Transport Properties of Rocks*, edited by B. Evans and T.-F. Wong, pp. 89–117, Elsevier, New York.

Turner, F. J., D. T. Griggs, and H. C. Heard (1954), Experimental deformation of calcite crystals, *Geol. Soc. Am. Bull.*, *65*, 883–934.

Weiss, J., and D. Marsan (2003), Three-dimensional mapping of dislocation avalanches: Clustering and space/time coupling, *Science*, *299*, 89–92.

Wibberley, C. A. J., and T. Shimamoto (2003), Internal structure and permeability of major strike-slip fault zones: The median tectonic line in Mie Prefecture, southwest Japan, *J. Struct. Geol.*, *25*, 59–78.

Zhang, S., S. F. Cox, and M. S. Paterson (1994), The influence of room temperature deformation on porosity and permeability in calcite aggregates, *J. Geophys. Res.*, *99*, 15,761–15,778.

J. Fortin and Y. Guéguen, Laboratoire de Geologie, Ecole Normale Superieure, 24, rue Lhomond, F-75231 Paris, France.

A. Schubnel B. D. Thompson, and R. P. Young, Lassonde Institute, University of Toronto, 170 College Street, Toronto, ON, Canada M5S 3E3. (alexandre.schubnel@utoronto.ca)

E. Walker, Ecole et Observatoire des Sciences de la Terre, 5 rue René Descartes, F-67084 Strasbourg, France.